Ligand Binding Dynamics to the Heme Domain of the Oxygen Sensor Dos from *Escherichia coli*

Ursula Liebl,[‡] Latifa Bouzhir-Sima,[‡] Laurent Kiger,[§] Michael C. Marden,[§] Jean-Christophe Lambry,[‡] Michel Négrerie,[‡] and Marten H. Vos*[,‡]

Laboratory for Optical Biosciences, INSERM U451, CNRS UMR 7645, Ecole Polytechnique-ENSTA, 91128 Palaiseau Cedex, France, and INSERM U473, 84 rue de General Leclerc, 94276 Le Kremlin Bicètre Cedex, France

Received December 13, 2002; Revised Manuscript Received March 13, 2003

ABSTRACT: In the heme-based oxygen sensor Dos from *Escherichia coli*, one of the axial ligands (Met 95) of a six-coordinate heme can be replaced by external ligands such as O_2, NO, and CO, which causes a switch in phosphodiesterase activity. To gain insight into the bidirectional switching mechanism, we have studied the interaction of ligands with the sensor domain DosH by flash photolysis experiments with femtosecond time resolution. The internal ligand can be photodissociated from the ferrous heme and recombines with time constants of 7 and 35 ps. This is somewhat slower than recombination of the external ligands NO, with which picosecond rebinding occurs with unprecedented efficiency (>99%) with a predominant phase of ∼5 ps, and O_2 (97% in 5 ps, Liebl, U., Bouzhir-Sima, L., Négrerie, M., Martin, J.-L., and Vos, M. H. (2002) *Proc. Natl. Acad. Sci. U.S.A. 99*, 12771−12776). Dissociated CO displays geminate rebinding in 1.5 ns with a very high yield (60%). Together these results indicate that the heme environment provides a very tight pocket for external ligands, presumably preventing frequent switching events. Additional CO dissociation and rebinding experiments on a longer time scale reveal that (a) Met 95 binding, in 100 μs, occurs in competition with bimolecular CO binding, and (b) subsequent replacement of Met 95 by CO on the millisecond time scale occurs faster than in rapid-mixing experiments, suggesting a slow further relaxation. A minimal ligand binding model is proposed that suggests that Met 95 displacement from the heme is facilitated by the presence of an external ligand in the heme environment. Furthermore, the orders of magnitude difference between Met 95 binding after dissociation of internal and external ligands, as well as the spectral characteristics of photodissociation intermediates, indicate substantial rearrangement of the heme environment associated with ligand sensing. Further remarkable observations include evidence for stable (>4 ns) photooxidation of six-coordinate ferrous heme, with a quantum yield of 4−8%.

Sensors of gaseous ligands initiate cascades of regulatory events involved in adaptation to changes in the environmental gas concentration. In recent years, a class of heme sensors has been characterized in which binding to and dissociation of small ligands, essentially carbon monoxide (CO) and oxygen (O_2), trigger molecular switches that eventually lead to modification of gene expression levels. The best-studied example is the rhizobial oxygen sensor FixL, which consists of a heme-binding PAS domain FixLH, and a histidine kinase domain (*1*−*5*). The activity of the latter domain is inhibited by binding of O_2 (and to a lesser extent CO and NO (*6*)) to the PAS domain. Here the heme is five-coordinate in the unliganded state, with histidine as the sole axial ligand, and six-coordinate when external ligands are bound (*1*, *7*−*11*). These features are the same as in the oxygen-storage protein myoglobin, but the ligand-binding properties of the two proteins are quite different. For instance, in FixL the O_2 affinity is much lower (*7*) and the exchange between protein-bound and solvent O_2 is much slower than in myoglobin, making it function as a "bistable switch" (*12*) in agreement with its function as a sensor.

Recently, Delgado-Nixon and co-workers (*13*) reported the characterization of DosH, a heme-binding PAS protein from *Escherichia coli* that has 60% sequence homology with FixLH, but is associated with a phosphodiesterase rather than a kinase regulatory domain. The functional role of this protein was also proposed to be oxygen sensing (*13*). Interestingly, despite the strong homology between FixLH and DosH, the heme coordination was found to be different. In all steady-state forms, the heme is six-coordinate, like in the CO-sensor protein CooA from *Rhodospirillum rubrum* (*14*, *15*) and a number of recently discovered hemoglobins with mostly yet uncertain function (*16*−*18*). For DosH, in the absence of external ligands, a methionine (Met 95) was proposed (*13*), and subsequently shown (*19*, *20*), to act as a second axial ligand. Thus, molecular oxygen must displace Met 95, and the transfer of the sensing perturbation is presumably different from that in FixL. Very recently, further spectroscopic and biochemical characterization studies of the Dos heme domain as well as the whole protein have been reported (*19*−*22*). In particular, in the full-length protein, apart from O_2, the activity of the regulatory domain was found to be

* Corresponding author. Phone: 33 1 69334777. Fax: 33 1 69333017. E-mail: Marten.Vos@polytechnique.fr.
‡ INSERM U451, CNRS UMR 7645, Ecole Polytechnique-ENSTA.
§ INSERM U473.

10.1021/bi027359f CCC: $25.00 © 2003 American Chemical Society
Published on Web 05/08/2003

influenced to a certain extent by CO and NO, and strongly by the oxidation state of the heme, which led to the suggestion that Dos might act as a redox sensor (*22*). The determination of a crystal structure of the heme domain is underway (*23*).

To understand the functioning of the sensing process, i.e., the pathway by which the perturbation induced by association or dissociation of oxygen is transferred within the heme domain, and the way different ligands are discriminated, intermediates in this process must be characterized. A powerful way to achieve this in heme proteins is to use time-resolved studies, in which the ligand dissociation reaction is synchronized by photodissociation from the heme. Using femtosecond absorption spectroscopy, we have indeed reported spectral evidence for intermediate heme-environment conformations after dissociation of ligands, and in particular O_2 from FixLH (*12*). In addition, the kinetics for CO and NO were myoglobin-like, but for O_2 extremely fast (~5 ps) and efficient (90%) rebinding was observed, which led us to propose that the heme environment acts as a ligand-specific trap. Even more efficient heme−O_2 recombination was observed for DosH (*12*). Here we report femtosecond to nanosecond spectroscopic studies of dissociation and rebinding of the external ligands CO and NO, and the internal ligand Met 95, with DosH. Evidence for a very closed heme pocket was found from the relatively pronounced geminate recombination for CO and NO. The study was complemented with measurement of bimolecular binding of CO on a longer time scale. The ensemble of results, including in certain aspects unusual properties, is discussed in the context of the function of the protein.

MATERIALS AND METHODS

The heme-containing Dos PAS domain from *E. coli* was expressed and purified as described (*12*). All samples were prepared in 50 mM Tris-HCl, pH 7.4. For the ultrafast measurements, gastight optical cells with an optical path length of 1 mm were used, and the protein concentration was adjusted to ~60 μM. The degassed as-prepared (ferric) sample was reduced with excess sodium dithionite to obtain the reduced nonliganded form (deoxy). To obtain the carbonmonoxy form, the deoxy form was equilibrated with 1 atm CO. To obtain the nitrosyl form, ferric DosH was reduced with 25 mM dithiothreitol and subsequently equilibrated with 0.1 atm NO. The reduction and ligandation of the different forms were monitored by the visible absorption spectrum, using a Shimadzu UV−Vis 1601 spectrophotometer.

Multicolor femtosecond absorption spectroscopy, using 30-fs pump pulses centered at 563 nm and white light continuum probe pulses, and data analysis in terms of decay associated spectra (DAS) were performed as described (*12*). The laser repetition rate was 30 Hz. The beams were focused to ~50 μm (illumination volume ~2 nL) and the sample was continuously moved perpendicular to the beams to ensure sample renewal between shots. The pulse energy was adapted to excite ~20% of the illumination volume. All experiments were carried out at room temperature.

CO bimolecular recombination kinetics in the micro- and millisecond time range were measured at a detection wavelength of 436 nm, after flash photolysis with 10 ns YAG laser pulses of 160 mJ at 532 nm (Quantel, France). For these measurements, degassed dithionite-reduced samples were equilibrated under CO at various concentrations in 1- or 4-mm optical cells. For each curve, at least 10 measurements were averaged, with at least 4 s between photolysis pulses to allow sample recovery.

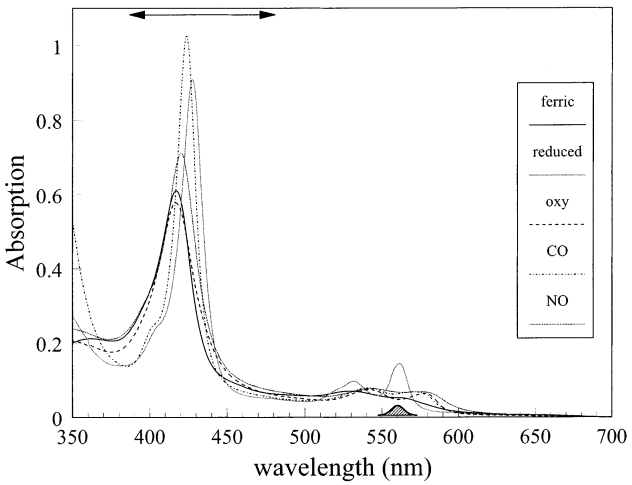

FIGURE 1: Ground-state absorption spectra of the different forms of DosH used in this study. The spectra are normalized to the same concentration. The spectral profile of the pump pulse and the probe region in the transient absorption experiments are indicated by the shaded area at the bottom and the bisided arrow, respectively.

The family of normalized curves was fitted together, with the same microscopic rate constants k_{CO}, k_{-CO}, k_M, and k_{-M} and ratio for differential extinction coefficients of the different transient species involved, to a model taking into account competitive binding of internal and external ligands (see Appendix). The fit function was calculated by numerical integration (MicroMath Scientist, Salt Lake City, UT) of equation (A2), under the conditions [Fe] = 1, [FeCO] = [FeMet95] = 0 at $t = 0$, and weighting the resulting population dynamics with the corresponding extinction coefficients.

RESULTS AND INTERPRETATION

Steady-state absorption spectra for the different ligation and redox states of DosH used in this study are shown in Figure 1, along with the spectrum of oxy-DosH (*12*). The spectra are very similar to those published previously (*13*, *22*) and reflect that for all states the steady-state configuration of the heme is six-coordinate (*20*, *21*). Thus, five-coordinate spectra for the heme in DosH are not directly available. In the following, transient spectra obtained after photodissociation of ligands will be presented and discussed. As a model for five-coordinate spectra, the ferric and ferrous unliganded spectra of FixLH (*7*, *12*) will be used to generate "steady-state" difference spectra for comparison. The Soret band of deoxy FixLH is very close to that of the DosH Met95 → Ile mutant (*1*, *19*), and similarly the generated FixLH unliganded *minus* DosH CO-liganded difference spectrum (see Figure 4 below) is very similar to the published M95I DosH deoxy *minus* CO-liganded spectrum (*19*), indicating that this approach is reasonable. The time-resolved measurements consist of excitation of the heme in its lowest lying transition (α band) and probing the excited state and ligand rebinding kinetics in the Soret band (Figure 1).

Ferric DosH. Figure 2A shows transient spectra at various delay times after excitation of ferric DosH. At short delay

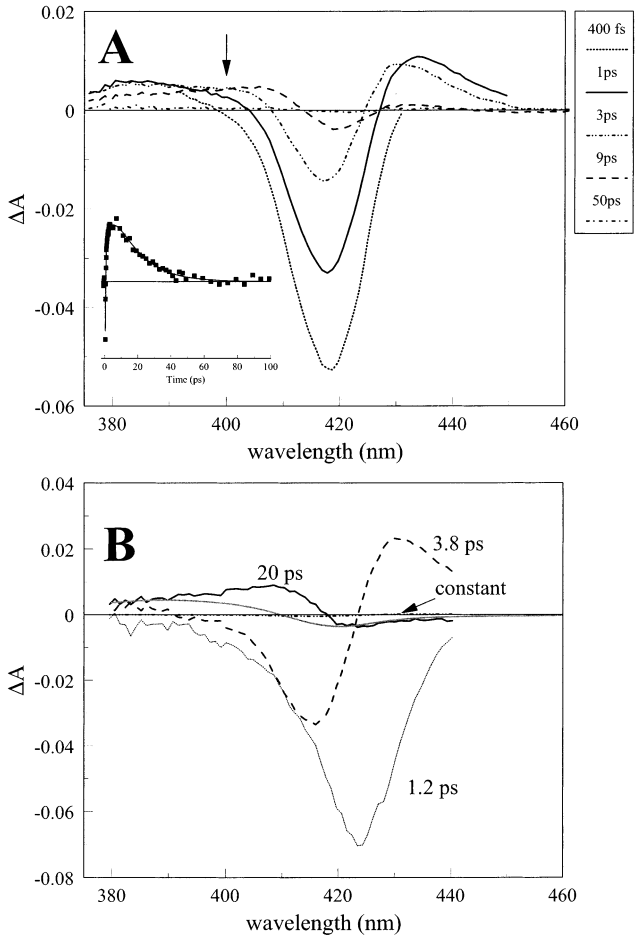

FIGURE 2: Photophysics and ligand rebinding in ferric DosH. (A) Transient absorption spectra at various delay times. (B) Decay-associated spectra of the decay components >1 ps. The solid gray line represents the steady-state FixLH minus DosH difference spectrum for the respective ferric forms, normalized on the bleaching part of the 20-ps DAS. Inset in A: kinetics at 400 nm (t > 400 fs).

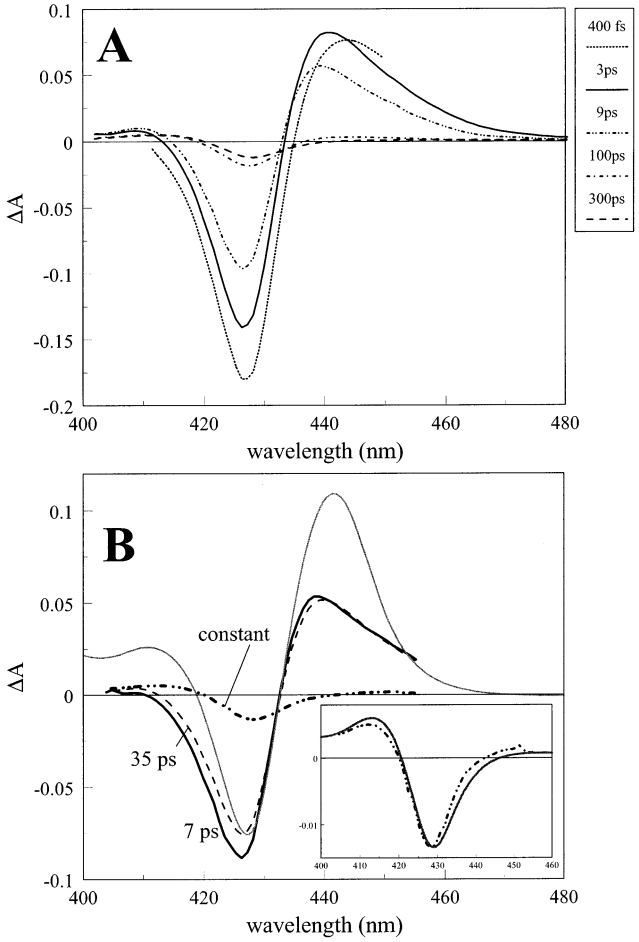

FIGURE 3: Photophysics and ligand rebinding in reduced DosH. (A) Transient absorption spectra at various delay times. (B) Decay-associated spectra of the decay components >3 ps. The solid gray line represents the steady-state FixLH minus DosH difference spectrum, for the respective reduced unliganded forms, normalized on the bleaching part of the 35-ps DAS. Inset: comparison of the constant phase (dash−dotted line) with the steady-state DosH oxidized minus reduced-unliganded spectrum (grey solid line), normalized at the bleaching part.

times, the spectra are dominated by the bleaching of the ground-state Soret band at ~418 nm and increased absorption at both the red and blue side of this band. The major part of the bleaching, and the red-side increased absorption, decay in a few picoseconds (see Figure 2B for an analysis in terms of DAS). Therefore, they can be ascribed to decaying excited states (cf. refs *12* and *24*).

The remaining spectrum (9-ps spectrum in Figure 2A) is characterized by a small bleaching around 420 nm and a broad increased absorption at the blue side, extending to below 380 nm. This spectrum decays to 0 with a time constant of 20 ps (Figure 2B). The characteristics of this phase are not indicative of excited states, which invariably display red induced absorption and decay faster (*25*). As the Soret absorption of five-coordinated ferric forms is at higher energy than the six-coordinated forms (*26*), a blue-shifted spectrum is consistent with dissociation of an axial ligand from the heme. Therefore, we suggest that the bond between the heme and Met 95 is dissociated in a fraction of the excited hemes. The 20-ps DAS is indeed roughly similar in shape to the steady-state five (FixLH) minus six (DosH)-coordinated difference spectrum (Figure 2B). The overall blue shift appears less extensive, however, possibly indicating a loosening rather than dissociation of the bond, or otherwise incomplete heme relaxation after dissociation. The disrupted bond is reestablished with a time constant of 20 ps.

Deoxy-DosH. Excitation of ferrous deoxy-DosH leads to spectral changes that are dominated by a strong red shift on the time scale up to ~100 ps (Figure 3A). Global analysis reveals several decay phases on the subpicosecond (not shown) and picosecond time scale (Figure 3B). The faster decay phases, with time constants of ~0.55 and ~2.3 ps (not shown), presumably reflect excited-state decay (*27*, *28*). The (red-shift) shape of the transient spectra remaining after the decay of these phases indicates the dissociation of an internal ligand from the heme. Indeed, the DAS of the picosecond decay phases (see below) shows resemblance with the steady-state FixLH (five-coordinate) minus DosH spectrum (Figure 3B). Therefore, these decay phases should reflect rebinding of the dissociated sixth ligand Met 95. The shape of the DAS is somewhat perturbed with respect to the model steady-state difference spectra; in particular, the induced absorption is relatively weak. This feature is also observed upon the dissociation of external ligands (see below and Discussion).

Using a multiexponential decay model, we found decay phases with time constants of 7 and 35 ps and very similar

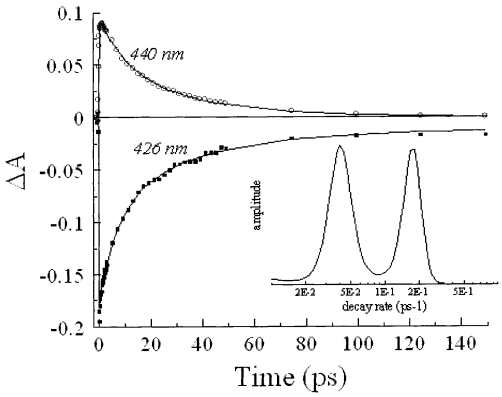

FIGURE 4: Transient kinetics of reduced DosH at 426 nm (lower trace) and 440 nm (upper trace). Inset: rate distribution obtained from a maximum entropy analysis of the 426-nm kinetics.

spectral properties (Figures 3B and 4), strongly indicating that they reflect the same process (i.e., methionine rebinding to heme). To discriminate between true biexponential decay and a distribution of decay rates, we also performed a kinetic analysis with a maximum entropy method (*29*) and found two clearly distinct rates (inset Figure 4). This strongly suggests that recombination occurs from two distinct conformations of the heme environment.

Intriguingly, after these decay phases, the ensemble of proteins has not returned to the initial six-coordinate state, as would be expected after recombination with an internal ligand. A small but significant spectral change persists (300-ps spectrum in Figure 3A) and does not decay within 4 ns (data not shown). This change has spectral characteristics that are very different from those of the picosecond decay phases: it consists of a *blue* shift rather than a red shift, implying that it does not reflect five-coordinate heme. Moreover, it cannot reflect a thermally excited heme, since (a) this would give rise to a red shift, and (b) the Soret band is known to be relatively temperature insensitive (*27*, *30*). The most likely candidate for a blue-shifted heme is ferric heme. The inset in Figure 3B shows that the long-lived spectral component corresponds remarkably well to a steady-state oxidized *minus* reduced difference spectrum of (six-coordinate) DosH. Therefore, we assign this feature to photooxidation of the heme. Assuming the 7- and 35-ps phases together represent 100% recombination of the methionine, and using the steady-state reduced-unliganded FixLH *minus* DosH and DosH oxidized *minus* reduced spectra as model spectra, we estimate that the quantum yield of the heme oxidation is 4−8% (depending on the normalization of the FixLH minus DosH spectrum and the DAS of the 7- and 35-ps phases). It remains to be determined whether intraprotein charge recombination occurs on a time scale >4 ns. We note that our experimental conditions (sample renewal between shots, low excitation energy, and excess reductant) prevent net photooxidation of the sample.

DosH−NO. As with other ligation states, excitation of DosH−NO leads to spectral changes on the time scale of ~1 ps that can be ascribed to excited state dynamics. On the time scale >3 ps the shape of the spectra does not change (Figure 5) and presumably reflects NO-dissociated heme. Comparison with the steady-state difference spectra indicates that the heme is five-coordinate, rather than six-coordinate, but the transient spectra are perturbed somewhat with respect

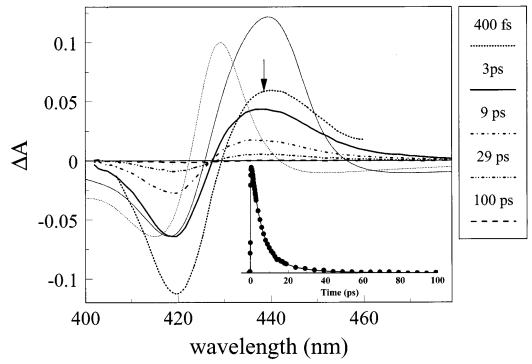

FIGURE 5: Ligand rebinding of NO with DosH. Transient absorption spectra at various delay times are shown. The gray lines represent the steady-state DosH unliganded minus DosH NO-liganded (dashed) and FixLH unliganded minus DosH NO-liganded (solid) spectra normalized on the bleaching part of the 3-ps transient spectrum. Inset: kinetics at the induced aborption maximum (438 nm).

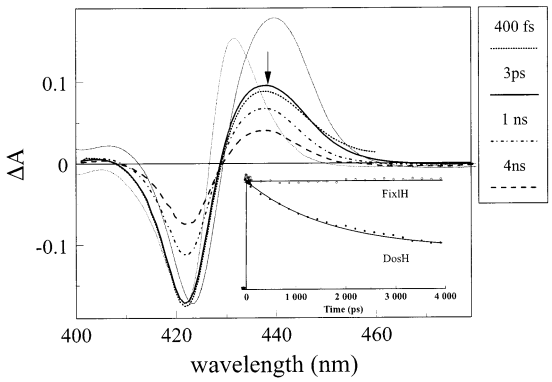

FIGURE 6: Ligand rebinding of CO with DosH. Transient absorption spectra at various delay times are shown. The gray lines represent the steady-state DosH unliganded minus DosH CO-liganded (dashed) and FixLH unliganded minus DosH CO-liganded (solid) spectra normalized on the bleaching part of the 3-ps transient spectrum. Inset: kinetics at the induced absorption maximum (438 nm) compared to the corresponding kinetics of FixLH−CO (439 nm).

to the "model" steady-state FixLH unliganded minus DosH NO-liganded difference spectrum, as observed previously, in a stronger way, for O_2 dissociation from DosH (*12*).

In DosH, NO rebinds to the heme in an extremely fast and efficient way (Figure 5, inset). As in most ligand-binding heme proteins (*12*, *31*−*34*), the recombination of NO with the heme was found to be nonexponential. Global analysis in terms of a multiexponential decay model resulted in time constants of 5 ps (85%) and 20 ps (15%) with very similar spectral characteristics (not shown), whereas the overall decay amounts to >99%. Thus, rebinding of NO occurs significantly faster than rebinding of the internal ligand methionine (see above). Also, the efficiency of NO rebinding on the picosecond time scale is higher than that reported for all other heme proteins, including the NO receptor guanylate cyclase (97% of monoexponential rebinding in 7.5 ps) (*35*).

DosH−CO. Transient spectra after dissociation of CO from DosH are shown in Figure 6. Small spectral evolutions take place on the time scale of a few picoseconds and less; these are presumably related to excited-state dynamics (*27*). The transient spectra on the picosecond time scale indicate formation of CO-dissociated heme. As with the NO-bound and deoxy transient spectra, the transient spectra are perturbed somewhat with respect to the "model" steady-state

Table 1: Decay Phases of Geminate and Internal Ligand Recombination of Different Redox and Ligation Forms of DosH[a]

	decay phase	rel. ampl.	assignment
ferric	20 ps		rebinding of a fraction of dissociated Met 95
deoxy	7 ps	0.53	rebinding of dissociated Met 95
	35 ps	0.47	
	>4 ns		partial heme oxidation
CO	1.5 ns	0.60	geminate recombination
	>4 ns	0.40	CO escape from protein
NO	5 ps	0.85	geminate recombination
	20 ps	0.15	
	>4 ns	0	
O_2[b]	5.3 ps	0.96	geminate recombination
	>4 ns	0.04	O_2 escape from protein

[a] Asymptotic phases in the ultrafast experiments are indicated as ">4 ns". [b] Ref *12*.

FixLH unliganded *minus* DosH CO-liganded difference spectrum (see Discussion).

No significant further spectral evolution takes place on the time scale up to a few hundred picoseconds, but on the nanosecond time scale substantial decrease of the signal is observed. This contrasts with the situation in most other heme proteins, and in particular in FixLH, where geminate rebinding of CO usually does not or hardly occur. Our data can be fit with a single-exponential decay with a time constant of 1.5 ns and amplitude of ~60% (the remaining 40% decays on a time scale beyond the temporal window of the pump−probe apparatus, see below). The *shape* of the transient spectrum does not change up to 4 ns, which implies that the coordinating of the CO-dissociated hemes does not change up to this time, consistent with nanosecond resonance Raman data (*20*).

In recent transient resonance Raman data on DosH, no indication for CO rebinding was found up to 1 ns (*20*). We are able to assess significant decay on this time scale (Figure 5, inset) due to the longer time window and possibly the higher signal-to-noise ratio allowed with transient absorption measurements. Our finding of 60% geminate recombination of CO with the heme implies that the *quantum yield* of CO diffusion out of the protein upon photodissociation does not exceed 40%. We note that multiple excitations within a flash longer than the 1.5 ns recombination time allow higher yields *per flash*. Indeed, Gonzalez and co-workers (*19*), using intense 6-ns flashes, reported as much as 80% CO dissociation on the microsecond time scale.

The ensemble of picosecond−nanosecond kinetic data on ligand rebinding in DosH is summarized in Table 1.

Microsecond Spectroscopy of DosH−CO. The heme rebinding kinetics upon photodissociation of CO from DosH on a longer time scale, monitored at 436 nm, are shown in Figure 7. They exhibit a typical biphasic pattern, with the rates of the fast (~100 μs) and the slow (millisecond) phases depending moderately and strongly, respectively, on the CO concentration. The relative amplitude of the fast phase increases with increasing CO concentration. Therefore, we assign this phase to competitive binding of the internal (Met 95) and external (CO) ligands; the overall rate involving the sum of the ligand association rates. This assignment differs somewhat from that of Gonzalez and co-workers (*19*), based on similar experiments on a more limited time window. They

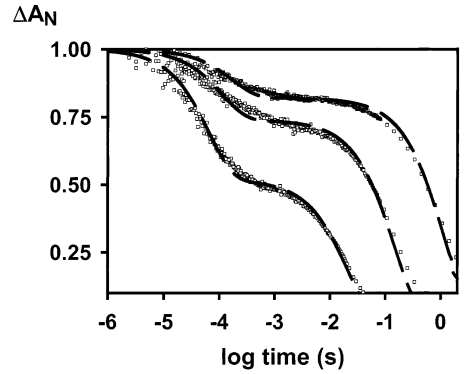

FIGURE 7: Normalized transient absorption after CO dissociation from DosH on the microsecond to second time scale, monitored at $\lambda = 436$ nm. The CO concentration in the measuring solution was 10 μM (upper), 100 μM (middle), and 1 mM (lower). Note that for hexacoordinate globins, the observed external ligand affinity K_{CO} at equilibrium depends on the competition with the internal ligand and therefore $K_{CO}(M^{-1}) = (k_{CO}/k_{-CO})/(1 + k_M/k_{-M})$.

attributed a phase of ~80 μs only to binding of the internal ligand, as the amplitude was reported to be independent of the CO concentration at the detection wavelength of 425 nm. The proximity of this wavelength to the isosbestic point between CO and methionine binding to the heme (*19*) and the fact that the slower, millisecond phase, was not recorded in these experiments presumably have prevented the assessment of a dependence of the amplitude of this phase, as clearly observed in the present work.

The millisecond phase, which is strongly CO concentration-dependent, is assigned to replacement of methionine by CO as the sixth heme ligand. The family of curves could be reasonably fitted together with the same rate constants k_{CO}, k_M, and k_{-M} (see Appendix, for low values of k_{-CO}, the fit is independent of this parameter) using the model, and the kinetic parameters of Figure 8A. The best simulation gives a value of 0.77 ± 0.05 for the ratio $\alpha_{436} = (\epsilon_{FeMet95} - \epsilon_{FeCO})/(\epsilon_{Fe} - \epsilon_{FeCO})$ of the extinction coefficients ϵ at 436 nm for the involved difference spectra. When comparing this value to that expected from the difference between the steady-state spectrum of reduced unliganded of FixLH (as a model spectrum for the pentacoordinate unliganded form ϵ_{Fe}) and DosH−CO, we find a value of $\alpha_{436} = 0.42$. However, using the unliganded minus CO-liganded difference spectrum that we observe at 4 ns (Figure 6), we find a value of $\alpha_{436} = 0.72$. This latter value is much closer to the value found from fitting the microsecond and millisecond data, therefore strongly indicating that the heme environment has not evolved to an equilibrium pentacoordinate conformation close to that of FixLH (and to that of the M95I mutant of DosH, which has a very similar spectrum (*1*, *19*)) on the microsecond time scale. Consistent with these findings, we could also reasonably simulate the transient spectra on the 50 μs to 1 ms time scale reported by Gonzalez and co-workers (*19*) with the static CO and deoxy spectra of *DosH* and the 4-ns pentacoordinate spectrum extracted from our fast kinetics (not shown).

The analysis yields a value of 1.0×10^4 s^{-1} for the intrinsic rate constant of Met 95 binding to CO-dissociated heme. This value is slightly lower than the value of 1.2×10^4 s^{-1} reported previously (*19*), due to the now assessed competition with CO binding, as discussed above. An important point is that this process is about 7 orders of magnitude slower than

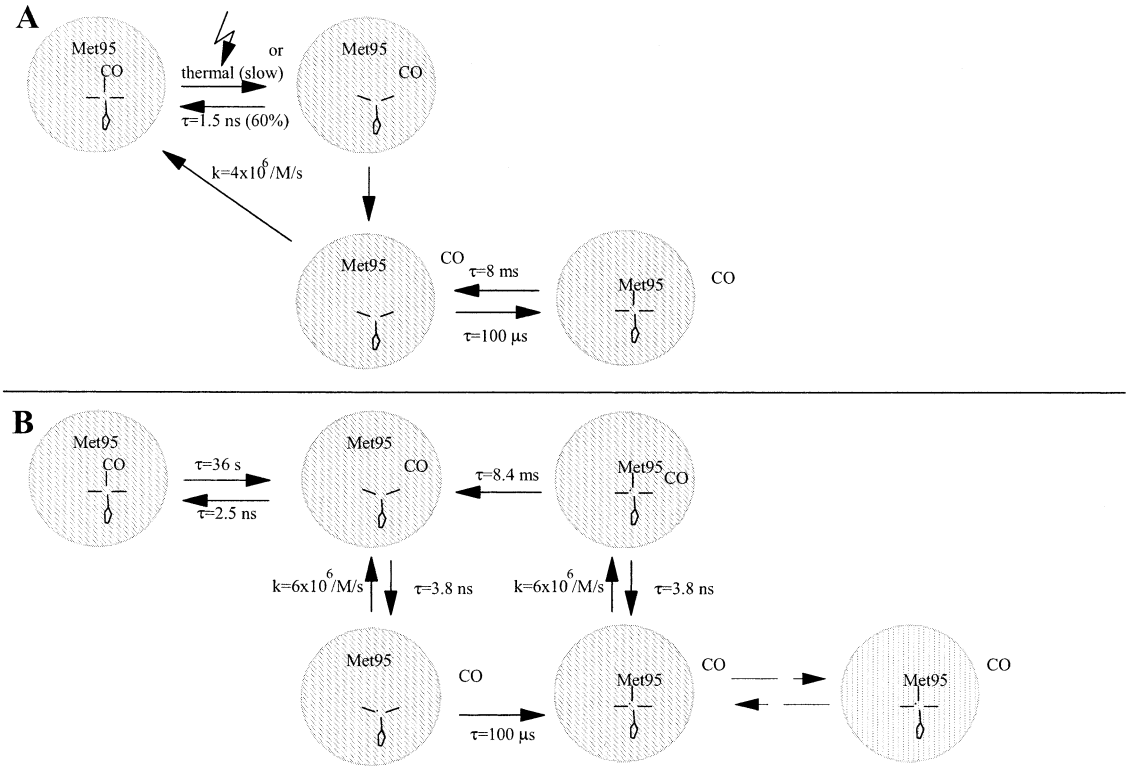

FIGURE 8: Schemes for CO and Met 95 binding with DosH. The protein moiety is represented by the hatched circles. (A) Summary of experimentally observed rate constants obtained from the ensemble of our CO-flash photolysis experiments. (B) Proposed scheme of microscopic rate constants consistent with the ensemble of our data. As discussed in the text, we propose that displacement of Met 95 from its heme-bound position occurs efficiently only in the presence of the (CO) external ligand near the heme pocket. The differently hatched protein representation at the lower right reflects a relaxed heme environment, invoked to explain the difference in bimolecular binding rates obtained with mixing experiments and with flash photolysis experiments.

Met 95 rebinding after Met 95 photodissociation (Figure 3), indicating substantial structural rearrangements in the heme pocket upon replacement of Met 95 by an external ligand (see Discussion).

Using flash photolysis, the bimolecular CO binding rate to hexacoordinated DosH is calculated to be $(k_{-M}/k_M)k_{CO} = 48 \times 10^3\ M^{-1}\ s^{-1}$. Interestingly, this is substantially higher than the values reported by single-wavelength stopped flow ($1.1 \times 10^3\ M^{-1}\ s^{-1}$ (*13*)). In addition, by rapid mixing experiments using a diode-array spectrophotometer (data not shown), we observed 3 times slower kinetics than the rate of binding predicted by the microscopic constants measured by flash photolysis on the same sample. This difference in flash photolysis and mixing-type experiments may indicate an additional slow protein relaxation after ligand release. This transition is tentatively indicated with dashed arrows in Figure 8B.

DISCUSSION

Our present results on the heme domain DosH complement our previous report including the DosH−O_2 complex (*12*) and have resulted in the assessment of a number of unusual properties of ligand dynamics. Some of these properties are clearly different from those previously assessed in the sensor domain FixLH (*12*).

Transient Spectra and Heme Coordination. For all external ligands studied (CO, NO, and O_2 (*12*)), dissociation of the six-coordinate ferrous heme initially leads to a spectrum that is consistent with a five-coordinate heme. Coordination with Met 95 was not observed before rebinding with the dissociated ligand on the picosecond time scale for NO and O_2 and, for CO, before the microsecond time scale ((*19*), see below). By contrast, dissociated Met 95 rebinds over 6 orders of magnitude faster (at slowest in ~35 ps, Figures 3 and 4), clearly implying the presence of intermediate conformation(s) in the heme environment after dissociation of CO and before formation of a near-equilibrium heme environment (see below). The presence of such intermediates can also be inferred from the transient *spectra* reported for CO and NO dissociation. These spectra, while inconsistent with a six-coordinate transient heme configuration, were found to be significantly disturbed with respect to the expected steady-state five-coordinate spectra, in a similar way as we previously observed for dissociation of ligands from FixLH (*12*). In particular, the reconstructed absolute spectra for the ligand-dissociated intermediates were found to be blue-shifted with respect to the "model" five-coordinate spectrum of FixLH in the order CO−NO−O_2 in a similar way as previously found for FixLH (not shown, cf. Figure 6 in ref *12*). The similarity with the transient spectra for FixLH suggests that similar structural elements in the heme pocket are involved, and that the (Dos-specific) Met 95 is far enough displaced from the heme not to strongly influence the heme spectrum in these ligand-dissociated intermediates. This observation is in general agreement with the much slower rebinding of Met 95 after dissociation of the external ligand (see below).

We note that qualitatively similar results of nonrebinding of the internal sixth ligand after dissociation of the external ligand CO were reported for the CO-sensor CooA (although a detailed spectral comparison was not made) (*28*), suggest-

ing that the presence of such intermediates in the heme environment is a universal feature for heme-based sensors.

Dynamics of External Ligands. The dynamics of geminate rebinding of the external ligands CO and NO was found to be more efficient than in FixLH. NO, which is known to have a very high affinity for heme, rebinds with time constants (5 and 20 ps) similar to those found for other heme proteins, including myoglobin (*31, 36*), guanylate cyclase (*35*), and FixLH (*12*). However, the yield of rebinding, >99%, is the highest known for the picosecond time scale, and indicates that NO essentially cannot escape from the heme pocket. CO does not rebind on the picosecond time scale, but shows a strong (60%) geminate recombination phase of 1.5 ns. After that in the CO-sensor protein CooA (*28*, *37*), this rebinding represents the most pronounced CO geminate recombination known in a monoheme protein. With the previously reported high yield of O_2 recombination (Table 1, (*12*)), the ensemble of data indicate that the heme pocket of DosH constitutes an extremely closed shelter for ligands, favoring the rebinding of ligands to the heme in a stronger fashion than for the homologous FixLH heme domain. These differences presumably are related to the observed lower ligand off-rates for DosH with respect to FixLH (*13*). The differences suggest that the heme pocket is not only modified with respect to FixLH in the deoxy, six-coordinate heme-ligation state (*19*), but also when the heme coordinates external ligands. The molecular origin of these differences remains to be explored by spectroscopic studies of mutants. Apart from Met 95 (Ile in FixLH), one might speculate that the replacement of Leu 236 in FixLH to Phe 113 in DosH, as deduced from the sequence alignment of ref *19*, induces steric modifications in the heme pocket.

CO Rebinding. Our studies on CO dissociation and rebinding cover a time span from femtoseconds to seconds, and include geminate rebinding, internal ligand binding, and ligand replacement phases. The ensemble of the results allows elaborating a minimal scheme of microscopic rates associated with these processes (Figure 8B). Briefly, dissociated CO rebinds to heme (2.5 ns) or diffuses out of the protein (3.8 ns). We cannot exclude that additional geminate rebinding occurs on a time scale of $\sim 10^{-7}$ s, but the high microsecond photodissociation yield suggests that such rebinding would not be substantial. Met 95 binds to the heme in 100 μs, at high CO concentration in competition with CO diffusion into the protein (6×10^6 M^{-1} s^{-1}) and subsequent binding to the heme. We suppose that the kinetics of CO moving in to and out of the protein are similar whether Met 95 is bound to the heme or not, but that Met 95 can only be detached sufficiently long to allow CO binding when CO is present near the heme. The latter proposal is inspired by the observed very fast rebinding of dissociated Met 95 in the absence of external ligands (Figure 3), and suggests that the presence of CO (or O_2) near the heme acts as a molecular "wedge" to displace Met 95. The time constant of dissociation of CO from the heme (36 s) is derived from the reported k_{off} of 0.011 s^{-1} (*13*) (combining our kinetic data with affinity measurements (not shown) we found a similar value) and the geminate recombination yield.

The difference in bimolecular CO binding to penta- and hexa- (Met 95) coordinate DosH indicate that in equilibrium, and in the absence of external ligands, >98% of the reduced hemes are hexacoordinate, in general agreement with characterizations by Raman spectroscopy (*20*, *21*). Finally, as indicated in Results, a further relaxation phase (depicted by a change in hatching of the protein moiety in Figure 8B) may take place on a longer time scale. Further studies on the heme domain as well as on the holoprotein should provide more insight into this putative transition and its possible functional role.

More generally, the scheme of Figure 8 may be useful to discuss the ensemble of ligand dynamics in hexacoordinate ligand-binding heme proteins and help to characterize their complex bimolecular ligand-binding properties (*16*, *38*, *39*). We note that the ensemble of kinetic phases observed in DosH is not necessarily always retrieved by flash photolysis experiments. For instance, in the bacterial CO-sensor CooA, the only other hexacoordinate heme protein for which both geminate and bimolecular ligand binding dynamics are presently available, internal ligand binding does not occur prior to CO rebinding (*40*).

Dissociation and Rebinding of the Intrinsic Sixth Axial Ligand. We have obtained strong indications that, in DosH, the bond of the ferric heme with the intrinsic sixth axial ligand, Met 95, is broken or at least weakened, in a fraction of the excited proteins (Figure 2). Whereas photodissociation of intrinsic axial ligands from ferrous hemes has been reported before (see below), this is to our best knowledge the first instance of such a process in a ferric heme. The bond is reestablished in ~20 ps, a similar time scale as rebinding of Met 95 upon dissociation from ferric heme (see below), which may suggest that the rebinding speed is not determined by electronic interactions, but rather by steric interactions.

Photodissociation of Met 95 was also observed from the ferrous heme (Figure 3); judging from comparison with the early transient spectra of CO and NO dissociation with near-unity quantum yield. Transient spectra have been interpreted in terms of dissociation of internal axial ligands from reduced heme previously, notably for the CO-sensor CooA (*28*), where the axial ligand is now known to be a proline (*41*), and for cytochrome *c* (*42*, *43*), where heme axial coordination is similar (His-Met) to DosH.[1] In both CooA and cytochrome *c* the dissociated ligand has been reported to rebind with a time constant of ~7 ps. In DosH, we found clear evidence for two distinct, but spectrally very similar, rebinding phases with roughly equal amplitudes (Figures 3 and 4) and time constants of 7 and 35 ps. This indicates that rebinding occurs from two conformations, presumably differing in methionine position or orientation, but with similar constraints on the heme. These conformations may be populated (a) sequentially in time, i.e., photodissociation initially leads to one dissociated-methionine conformation which decays, in 7 ps, in parallel back to a six-coordinate heme conformation and to a second dissociated-methionine conformation, which itself recombines in 35 ps or (b) in parallel, possibly reflecting two different conformations present already in the initial six-coordinate state. At present, we cannot discriminate between these two schemes. The assessment of different methionine-dissociated conformations close to the bound configuration

[1] The photon energies used in the cytochrome *c* studies (excitation in the blue and near-UV) were substantially higher than in our present study, where the excess energy was minimized by exciting in the lowest-lying optical transition of the heme, near 563 nm.

may be relevant for future determination of the way oxygen replaces methionine as a ligand. In this context, it is interesting to note that the rebinding of dissociated methionine occurs on a slower time scale than the rebinding of the dissociated external ligands O_2 (*12*) (and also NO). This suggests that upon (thermal) dissociation of methionine, O_2, once present near the heme pocket, could efficiently compete for binding to the heme. The presence of two distinct methionine-dissociated conformations could indicate a specific pathway for its motion away from the heme to accommodate an external ligand. Molecular dynamics studies on the basis of the forthcoming crystal structure (*23*) may help to clarify these issues.

The identified short-lived six-coordinate methionine-dissociated conformations of the heme pocket must be different from the configuration(s) obtained after dissociation of external ligands, where methionine binding to the heme does not occur on the picosecond time scale. Clearly, the presence of the external ligand near the heme prohibits methionine to approach the heme, but even after diffusion of dissociated CO out of the heme pocket methionine binding takes as long as ~100 μs. Altogether, the kinetic studies convey that major structural rearrangements, with multiple intermediate configurations, occur in the heme environment during the exchange of methionine and external ligands.

During none of the observed intermediates, including that on the microsecond time scale after CO dissociation but prior to methionine binding, the heme spectrum is close to that of the five-coordinate FixLH spectrum. This suggests that a FixL-like heme environment is never adopted. This observation is in general agreement with the assessment that in DosH for Met 95 to approach the heme iron, the heme domain must be substantially distorted with respect to FixLH (*19*), and indicates that this distortion influences the heme configuration even when Met 95 is not ligated to the heme. In the same line, using molecular dynamics methods, we have attempted to construct a model of the DosH structure using the crystal structure of FixLH (*8*) as a template. Whereas the general PAS domain structure is well conserved with this approach, complications arise when modeling the distal heme environment due to the substantial rearrangements imposed by the introduction of a bond between the heme iron and the methionine sulfur atoms.

Electron Transfer. Our data show a quite unexpected feature in the relatively stable (>4 ns) reduction of the ferrous heme upon excitation of the reduced deoxy protein (Figure 3). We are not aware of any other example of direct photooxidation of hemes in a heme protein. The low quantum yield (4−8%) of the process prevents us from establishing whether oxidation occurs directly from the excited state or after recombination of the dissociated methionine. The corresponding electron acceptor has not been identified; one might speculate on the possibility that the electron initially resides on the dissociated methionine and can be transferred to a subsequent electron acceptor prior to rebinding. Whatever the mechanism, our observation is interesting in light of the recently reported and possibly physiologically relevant inactivation of the Dos regulatory domain by ferric heme in the heme domain (*22*). Combining these observations indicates that optical spectroscopic techniques may also be used to study the molecular mechanism of this inactivation, and, in extremis, might even imply that Dos can act as a light sensor.

Concluding Remarks. We have presented a survey of the dynamics of intrinsic and three different external ligands after dissociation from DosH. We provided evidence for several intermediates which can be significantly populated by flash photolysis and for which it will be useful to further determine the characteristics using time-resolved vibrational techniques. A common feature emerging from the ensemble of data on DosH is that recombination with external ligands occurs with a very high speed and yield (for NO even 100%), indicating a very confined heme pocket. In another heme-based sensor where the sensed ligand replaces an internal heme axial ligand, CooA, a similar feature was observed (at least with the physiological ligand CO) (*28*). Thus, it would appear that highly efficient recombination of external ligands is a general feature for ligand-binding six-coordinate proteins, an issue that can be addressed by ultrafast studies on other six-coordinate proteins (*16*−*18*). These studies may also help to characterize the complex bimolecular ligand-binding properties in these proteins (*38*, *39*).

The phosphodiesterase activity of reduced Dos is inhibited by O_2, but, presumably to a lesser extent, also by CO and NO (*22*). The relatively high yield of CO dissociation on the time scale beyond picoseconds may make the CO-bound form of Dos the best adapted model to study the molecular mechanism of the *release* of the inhibition. With this prospect, we have developed a minimal CO binding scheme from the ensemble of data available on the femtosecond to second time scale. However, the heme-based sensors can be regarded as bistable switches (*12*), and the mechanisms of the transitions in both directions are physiologically relevant. Our results indicate that, in Dos, the regulatory mechanism may also be tackled starting from the other position of the switch, as at least the early intermediates of the *onset* of inhibition may be populated by dissociation of the internal methionine ligand.

APPENDIX

The microsecond/millisecond data are analyzed in terms of a model involving three ligation states of the heme, the CO-bound hexacoordinate state FeCO, the pentacoordinate state Fe and the Met95-bound hexacoordinate state FeMet95. This is a simplified scheme of that presented in Figure 8A, excluding the (faster) geminate phases,

$$\mathrm{FeCO} \underset{k_{\mathrm{CO}}}{\overset{k_{-\mathrm{CO}}}{\rightleftharpoons}} \mathrm{Fe} \underset{k_{-\mathrm{M}}}{\overset{k_{\mathrm{M}}}{\rightleftharpoons}} \mathrm{FeMet95} \qquad \text{(A1)}$$

in which k_{CO} and $k_{-\mathrm{CO}}$ are the bimolecular rate of CO binding to the pentacoordinate heme, iron and the (thermal) CO dissociation rate, respectively, and k_{M} and $k_{-\mathrm{M}}$ are the rates for Met 95 binding and dissociation, respectively. The corresponding set of coupled differential equations reads:

$$\frac{d[\mathrm{FeCO}]}{dt} = k_{\mathrm{CO}}[\mathrm{Fe}][\mathrm{CO}] - k_{-\mathrm{CO}}[\mathrm{FeCO}] \qquad \text{(A2a)}$$

$$\frac{d[\mathrm{Fe}]}{dt} = -k_{\mathrm{CO}}[\mathrm{Fe}][\mathrm{CO}] + k_{-\mathrm{CO}}[\mathrm{FeCO}] - k_{\mathrm{M}}[\mathrm{Fe}] + k_{-\mathrm{M}}[\mathrm{FeMet95}] \qquad \text{(A2b)}$$

$$\frac{d[\mathrm{FeMet95}]}{dt} = -k_{-\mathrm{M}}[\mathrm{FeMet95}] + k_{\mathrm{M}}[\mathrm{Fe}] \qquad \text{(A2c)}$$

Note that the solvent CO concentration [CO] is usually the equilibrium value $[CO]_{eq}$ depending on the gas partial pressure and solubility coefficient; however, at low CO levels one must take into account the CO photodissociated from the protein which varies in time and depends on the fraction (f) of protein bound with CO:

$$[CO] = [CO]_{eq} + [protein]\,(1 - f[FeCO]) \quad \text{(A3)}$$

For constant CO concentrations, solving the set of equations (A2) yields biexponential kinetics for the population dynamics of the three species. For $k_{-CO} \ll k_M$, $k_{-M}k_{CO}[CO]$, as is the case in DosH (see Discussion), the two observed rates k_1 and k_2 read:

$$k_{1,2} = k_M + k_{-M} + k_{CO}[CO] \pm \sqrt{(k_M + k_{-M} + k_{CO}[CO])^2 - 4(k_{-M}k_{CO}[CO])}/2 \quad \text{(A4)}$$

It is straightforward to show that for the conditions [Fe] = 1, [FeCO] = [FeMet95] = 0 at $t = 0$, and with extinction coefficients ϵ_{FeCO}, ϵ_{Fe}, and $\epsilon_{FeMet95}$ for the three different species, the overall transient absorption kinetics are of the form:

$$\Delta A(t) \sim \frac{1}{k_1 - k_2}(((\epsilon_{Fe} - \epsilon_{FeCO})(k_1 - k_{-M}) - (\epsilon_{FeMet95} - \epsilon_{FeCO})k_M)e^{-k_1 t} + (\epsilon_{Fe} - \epsilon_{FeCO})(k_{-M} - k_2) + (\epsilon_{FeMet95} - \epsilon_{FeCO})k_M)e^{-k_2 t}) \quad \text{(A5)}$$

REFERENCES

1. Gilles-Gonzalez, M. A., Ditta, G. S., and Helinski, D. R. (1991) *Nature 350*, 170−172.
2. Perutz, M. F., Paoli, M., and Lesk, A. M. (1999) *Chem. Biol. 6*, R291−R297.
3. Rodgers, K. R. (1999) *Curr. Opin. Chem. Biol. 3*, 158−167.
4. Pellequer, J.-L., Brudler, R., and Getzoff, E. D. (1999) *Curr. Biol. 9*, R416−R418.
5. Gilles-Gonzalez, M. A. (2001) *IUBMB Life 51*, 165−173.
6. Tuckerman, J. R., Gonzalez, G., Dioum, E. M., and Gilles-Gonzalez, M. A. (2002) *Biochemistry 41*, 6170−6177.
7. Gilles-Gonzalez, M. A., Gonzalez, G., Perutz, M. F., Kiger, L., Marden, M. C., and Poyart, C. (1994) *Biochemistry 33*, 8067−8073.
8. Gong, W., Hao, B., Mansy, S. S., Gonzalez, G., Gilles-Gonzalez, M. A., and Chan, M. K. (1998) *Proc. Natl. Acad. Sci. U.S.A. 95*, 15177−15182.
9. Gong, W., Hao, B., and Chan, M. K. (2000) *Biochemistry 39*, 3955−3962.
10. Miyatake, H., Mukai, M., Park, S.-Y., Adachi, S., Tamura, K., Nakamura, H., Nakamura, K., Tsuchiya, T., Iizuka, T., and Shiro, Y. (2000) *J. Mol. Biol. 301*, 415−431.
11. Hao, B., Isaza, C., Arndt, J., Soltis, M., and Chan, M. K. (2002) *Biochemistry 41*, 12952−12958.
12. Liebl, U., Bouzhir-Sima, L., Négrerie, M., Martin, J.-L., and Vos, M. H. (2002) *Proc. Natl. Acad. Sci. U.S.A. 99*, 12771−12776.
13. Delgado-Nixon, V. M., Gonzalez, G., and Gilles-Gonzalez, M. A. (2000) *Biochemistry 39*, 2685−2691.
14. Aano, S., Nakajima, H., Saito, K., and Okada, M. (1996) *Biochem. Biophys. Res. Comm. 228*, 752−756.
15. Shelver, D., Kerby, R. L., He, Y., and Roberts, G. P. (1997) *Proc. Natl. Acad. Sci. U.S.A. 94*, 11216−11220.
16. Dewilde, S., Kiger, L., Burmester, T., Hankeln, T., Baudin-Creuza, V., Aerts, T., Marden, M. C., Caubergs, R., and Moens, L. (2001) *J. Biol. Chem. 276*, 38949−38955.
17. Trent, J. T., III., and Hargrove, M. S. (2002) *J. Biol. Chem. 277*, 19538−19545.
18. Hankeln, T., Jaenicke, V., Kiger, L., Dewilde, S., Ungerechts, G., Schmidt, M., Urban, J., Marden, M. C., Moens, L., and Burmester, T. (2002) *J. Biol. Chem. 277*, 29012−29017.
19. Gonzalez, G., Dioum, E. M., Bertolucci, C. M., Tomita, T., Ikeda-Saito, M., Cheesman, M. R., Watmough, N. J., and Gilles-Gonzalez, M. A. (2002) *Biochemistry 41*, 8414−8421.
20. Sato, A., Sasakura, Y., Sugiyama, S., Sagami, I., Shimizu, T., Mizutani, Y., and Kitagawa, T. (2002) *J. Biol. Chem. 277*, 32650−32658.
21. Tomita, T., Gonzalez, G., Chang, A. L., Ikeda-Saito, M., and Gilles-Gonzalez, M. A. (2002) *Biochemistry 41*, 4819−4826.
22. Sasakura, Y., Hirata, S., Sugiyama, S., Suzuki, S., Taguchi, S., Watanabe, M., Matsui, T., Sagami, I., and Shimizu, T. (2002) *J. Biol. Chem. 277*, 23821−23827.
23. Park, H., Suquet, C., Savenkova, M. I., Satterlee, J. D., and Kang, C. H. (2002) *Acta Crystallogr. D58*, 1504−1506.
24. Borisov, V. B., Liebl, U., Rappaport, F., Martin, J.-L., Zhang, J., Gennis, R. B., Konstantinov, A. A., and Vos, M. H. (2002) *Biochemistry 41*, 1654−1662.
25. Martin, J.-L., and Vos, M. H. (1994) *Methods Enzymol. 232*, 416−430.
26. Wood, P. M. (1984) *Biochim. Biophys. Acta 768*, 293−317.
27. Petrich, J. W., Poyart, C., and Martin, J.-L. (1988) *Biochemistry 27*, 4049−4060.
28. Kumazaki, S., Nakajima, H., Sakaguchi, T., Nakagawa, E., Shinahara, H., Yoshihara, K., and Aano, S. (2000) *J. Biol. Chem. 275*, 38378−38383.
29. Steinbach, P. J., Ansari, A., Berendzen, J., Braunstein, D., Chu, K., Cowen, B. R., Ehrenstein, D., Frauenfelder, H., Johnson, J. B., Lamb, D. C., Luck, S., Mourant, J. R., Nienhaus, G. U., Ormos, P., Philipp, R., Xie, A., and Young, R. D. (1991) *Biochemistry 30*, 3988−4001.
30. Schomaker, K. T., Bangcharoenpaurpong, O., and Champion, P. M. (1984) *J. Chem. Phys. 80*, 4701−4717.
31. Petrich, J. W., Lambry, J.-C., Kuczera, K., Karplus, M., Poyart, C., and Martin, J.-L. (1991) *Biochemistry 30*, 3975−3978.
32. Petrich, J. W., Lambry, J.-C., Balasubramanian, S., Lambright, D. G., Boxer, S. G., and Martin, J.-L. (1994) *Biochemistry 238*, 437−444.
33. Carlson, M. L., Regan, R., Elber, R., Li, H., Phillips, G. N., Jr., Olson, J. S., and Gibson, Q. H. (1994) *Biochemistry 33*, 10597−10606.
34. Walda, K. N., Liu, X. Y., Sharma, V. S., and Magde, D. (1994) *Biochemistry 33*, 2198−2209.
35. Négrerie, M., Bouzhir-Sima, L., Martin, J.-L., and Liebl, U. (2001) *J. Biol. Chem. 276*, 46815−46821.
36. Négrerie, M., Berka, V., Vos, M. H., Liebl, U., Lambry, J.-C., Tsai, A.-L., and Martin, J.-L. (1999) *J. Biol. Chem. 274*, 24694−24702.
37. Rubtsov, I. V., Zhang, T., Nakajima, H., Aano, S., Rubtsov, G. I., Kumazaki, S., and Yoshihara, K. (2001) *J. Am. Chem. Soc. 123*, 10056−10062.
38. Kriegl, J. M., Bhattacharyya, A. J., Nienhaus, K., Deng, P., Minkow, O., and Nienhaus, G. U. (2002) *Proc. Natl. Acad. Sci. U.S.A. 99*, 7992−7997.
39. Trent, J. T., III., Hvitved, A. N., and Hargrove, M. S. (2001) *Biochemistry 40*, 6155−6163.
40. Uchida, T., Ishikawa, H., Takahashi, S., Ishimori, K., Morishima, I., Ohkubo, K., Nakajima, H., and Aano, S. (1998) *J. Biol. Chem. 32*, 19988−19992.
41. Lanzilotta, W. N., Schuller, D. J., Thorsteinsson, M. V., Kerby, R. L., Roberts, G. P., and Poulos, T. L. (2000) *Nat. Struct. Biol. 7*, 876−880.
42. Jongeward, K. A., Magde, D., Taube, D. J., and Traylor, T. G. (1988) *J. Biol. Chem. 263*, 6027−6030.
43. Wang, W., Ye, X., Demidov, A. A., Rosca, F., Sjodin, T., Cao, W., Sheeran, M., and Champion, P. M. (2000) *J. Phys. Chem. B 104*, 10789−10801.

BI027359F